CHIN. PHYS. LETT. Vol. 36, No. 4 (2019) 044203

Temperature-Dependent Dielectric Characterization of Magneto-Optical $Tb_3Sc_2Al_3O_{12}$ Crystal Investigated by Terahertz Time-Domain Spectroscopy *

Ju-Geng Li(李炬赓)[1], Sen-Miao Yang(杨森淼)[1], Xin Chen(陈新)[2], Nai-Feng Zhuang(庄乃锋)[2], Qi-Biao Zhu(朱绮彪)[1], An-Hua Wu(武安华)[3], Xian Lin(林贤)[1], Guo-Hong Ma(马国宏)[1,4**], Zuan-Ming Jin(金钻明)[1,4**], Jian-Quan Yao(姚建铨)[5]

[1]*Department of Physics, College of Sciences, Shanghai University, Shanghai 200444*
[2]*College of Chemistry and Chemical Engineering, Fuzhou University, Fuzhou 350108*
[3]*Shanghai Institute of Ceramics, Chinese Academy of Science, Shanghai 200050*
[4]*STU & SIOM Joint Laboratory for Superintense Lasers and the Applications, Shanghai 201210*
[5]*College of Precision Instrument and Opto-electronics Engineering, Institute of Laser and Optoelectronics, Tianjin University, Tianjin 300072*

(Received 18 January 2019)

Terbium scandium aluminum garnet (TSAG) crystals have been widely used in magneto-optical systems. We investigate the complex refractive index of the TSAG crystal in the terahertz frequency range using terahertz (THz) time-domain spectroscopy in the temperature range 100–300 K. It is observed that the refractive index and the absorption coefficient increase with the THz frequency. The refractive index increases with the temperature. We measure the temperature coefficient of the refractive index of the TSAG crystal in the frequency range 0.4–1.4 THz. Furthermore, the loss tangent, i.e., the ratio of experimental values of the imaginary and real part of the dielectric permittivity, is found to be almost independent of frequency. TSAG is very promising for applications in THz optoelectronics because it has a high dielectric constant, low loss, and low thermal coefficient of the dielectric constant.

PACS: 42.25.Bs, 77.22.Ch, 78.20.Ci, 78.47.−p DOI: 10.1088/0256-307X/36/4/044203

Ultrafast magnetic phenomena in magneto-optical crystals triggered by femtosecond laser pulses have attracted great interest from both fundamental physics of magnetism and potential applications in spintronics.[1,2] Stupakiewicz *et al.* described the ultrafast all-optical photo-magnetic recording in transparent films of the dielectric cobalt-substituted garnet (YIG:Co). By changing the polarization of the laser pulse, the net magnetization in the garnet can be steered deterministically, thus writing magnetic bits 0 and 1.[3] Furthermore, Mikhaylovskiy *et al.* and Jin *et al.* separately reported the ultrafast inverse Faraday effect (IFE) in a paramagnetic terbium gallium garnet crystal $Tb_3Ga_5O_{12}$ (TGG).[4,5] Based on the IFE, Gorelov *et al.* reported terahertz (THz) Cherenkov radiation from a moving magnetic moment produced in TGG.[6,7] Recently, Subkhangulov *et al.* found a THz modulation of the magneto-optical Faraday effect in TGG, which is the result of the interaction of two counter-propagation laser pulses via the optical Kerr effect.[8,9]

In 1997, Riordan *et al.* used a free-space magneto-optic sampling sensor of TGG to measure the transient magnetic component of a freely propagating THz beam.[10] Recently, Qiu *et al.* reported a substantial enhancement of THz magnetic near field achieved by a combination of a tapered metallic waveguide and a micro-split-ring resonator. The magnetic near field is directly probed via the TGG crystal.[11] Kurihara *et al.* proposed and experimentally demonstrated that the THz magnetic near-field-detection sensitivity of magneto-optical sampling with the TGG crystal can be drastically enhanced by cooling the crystal down to cryogenic temperatures.[12]

Rare-earth garnet single crystals with large Faraday rotation angles and low optical absorption loss have been widely used for magneto-optical applications.[13−15] Recently, a new magneto-optical crystal of terbium scandium aluminum garnet (TSAG) was successfully designed and grown.[16−20] The Verdet constant of the TSAG crystal is about 20–25% higher than that of the traditionally used TGG crystal. The small thermo-optic constant makes the TSAG crystal used in high-average-power laser operations.[18] Numerous works have been reported on the growth of TSAG crystals with the mechanics and thermal properties,[17] while the temperature dependence of the permittivity of the TSAG crystal at THz frequencies is still inadequately demonstrated.[21,22] The permittivity is a fundamental property of materials, which is related to the electronic polarizability of ions, local field inside materials, and is important for the THz Cherenkov radiation.[6,7] In this work, our measurements are carried out using a THz time-domain spectroscopy (THz-TDS), which is a phase-sensitive measurement technique. THz-TDS can provide more information than conventional Fourier-transform infrared spectroscopy, by which a power spectrum is measured. THz-TDS is convenient and valuable to investigate the complex di-

*Supported by the National Natural Science Foundation of China under Grant Nos 11604202, 11674213, 61735010 and 51572275, the Shanghai Rising-Star Program under Grant No 18QA1401700, the 'Chen Guang' Project under Grant No 16CG45, the Shanghai Municipal Education Commission, and the Shanghai Education Development Foundation.
**Corresponding author. Email: physics_jzm@shu.edu.cn; ghma@staff.shu.edu.cn
© 2019 Chinese Physical Society and IOP Publishing Ltd

electric properties of materials without requiring the Kramers–Kronig relation.[23,24] The refractive index, absorption, as well as the complex permittivity, and loss tangent of the TSAG single crystal are determined over the temperature range 100–300 K and frequency range 0.4–1.4 THz. Furthermore, we extract the temperature coefficient τ_n as a function of THz frequency, indicating the relative change of the refractive index with temperature. The value of τ_n is given to be $(19.6 \pm 3.2) \times 10^{-6}\mathrm{K}^{-1}$@0.4 THz, which is decreasing to $(6.2 \pm 4.0) \times 10^{-6}\,\mathrm{K}^{-1}$@1.4 THz, demonstrating a low thermal coefficient of the dielectric constant for the TSAG crystal.

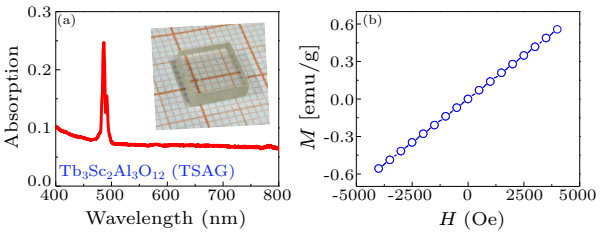

Fig. 1. (a) The absorption spectrum of the TSAG crystal. Inset: photo of the TSAG crystal with double-side polished. (b) The applied magnetic field dependence of magnetization response of the TSAG crystal.

The TSAG single crystal with dimensions of $8\times8\times3\,\mathrm{mm}^3$ was grown by the Czochralski method.[20] The inset in Fig. 1(a) shows the photograph of our TSAG crystal. The room-temperature absorption spectrum of the TSAG single crystal in the wavelength range of 400–800 nm is shown in Fig. 1(a). The high transmittance in the wavelength above 505 nm indicates that the crystal can be used as an effective optical Faraday isolation in the visible and near infrared regions. The absorption at 800 nm is much small, i.e., ∼0.06. There is a strong absorption peak at 487 nm, which corresponds to the f–f transition line ($^7F_6$ to $^5D_4$) of Tb^{3+} in the TSAG crystal. Figure 1(b) shows the magnetization curve M–H of the TSAG crystal, and it is clearly seen that the relationship between magnetization and applied magnetic field is linear, indicating a paramagnetic material. Additionally, no magnetic anisotropy is found within the in-plane of the sample.

A standard THz-TDS in transmission geometry was used to characterize the sample in the frequency range 0.4–2 THz. Briefly, the output of a mode-locked Ti:sapphire laser, with pulse duration of 100 fs, central wavelength 800 nm, and repetition rate 80 MHz (MaiTai HP, Spectra-Physics), is used to generate and detect the THz transient. The THz pulses are generated from LT-GaAs photoconductive antennas. The generated THz pulses are collimated into parallel beams by a micro silicon lens. The sample is positioned at the beam waist of the THz beam. After interacting with the sample investigated, the THz pulses are detected by a photoconductive switching. The photoconductive switch consists of a metallic dipole antenna on a small piece of a low-temperature (LT) grown GaAs with a sub-ps carrier lifetime. The photo-induced carriers of LT-GaAs are driven by the THz electromagnetic field, which produces a detected current. The THz field amplitude is proportional to the current pulse. By a variable optical delay, the THz pulses generated at the emitter can be continuously delayed with respect to the gated detector, which allows us to temporally scan their electric field with both the amplitude and the phase information, as shown in Fig. 2. The THz-TDS system is purged with dry N_2 gas to reduce the THz absorption due to residual water vapor in the beam path.

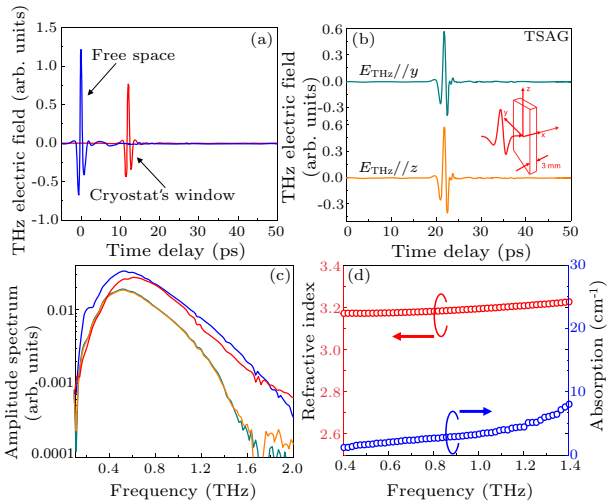

Fig. 2. (a) The transmitted THz pulses measured without the sample at room temperature. The THz pulse transmitted through air used as a reference (blue line) and through the windows of the cryostat (red line). (b) THz pulses through the TSAG crystal as the $E_{\mathrm{THz}} \parallel y$ and $E_{\mathrm{THz}} \parallel z$ axis. (c) Amplitude spectra in the frequency domain from the fast Fourier transformation of the transmission time-domain data. (d) Refractive index dispersion and absorption coefficient of the TSAG crystal at room temperature.

Figure 2(a) is a typical time-domain waveform (blue line) observed for dry N_2 at room temperature, taken as a reference, $E_{\mathrm{ref}}(t)$. Figure 2(b) represents the transmitted THz waveforms through the TSAG crystal with thickness of 3 mm in the time domain, taken as $E_{\mathrm{sample}}(t)$. Using the Fourier transforming, we obtained the spectrum of the reference signal $E_{\mathrm{ref}}(\nu)$ and the sample signal $E_{\mathrm{sample}}(\nu)$. As shown in Fig. 2(c), the spectral range of current setup extends from 0.4 to 1.4 THz. As shown in Figs. 2 (b) and 2(c), the phase delay and the attenuation of the THz electric field perpendicular and parallel to the z axis of the sample are almost the same. It is apparent that the complex refractive index within the range of 0.4–1.4 THz is independent of the polarization of THz wave along the in-plane directions. In contrast, the TSAG crystal has a high absolute value of the optical anisotropy parameter $\xi = -101 \pm 10$@1076 nm at room temperature.[25,26]

We assume a plane wave impinging on a layer of the thickness d at normal incidence. The transmittance is given by[27]

$$T(\nu) = \frac{\tilde{E}_{\mathrm{sample}}(\nu)}{\tilde{E}_{\mathrm{Ref}}(\nu)} = A(\nu)\exp(-i\Delta\phi)$$
$$= T_1(\nu)T_2(\nu)\cdot\exp\Big(-i\frac{(\tilde{n}(\nu)-1)2\pi\nu d}{c}\Big), \quad (1)$$

where $\tilde{n}(\nu)$ is the complex refractive index of the sample, c is the speed of light in vacuum, and $T_1(\nu) = \frac{2}{1+\tilde{n}(\nu)}$ and $T_2(\nu) = \frac{2\tilde{n}(\nu)}{1+\tilde{n}(\nu)}$ are the Fresnel transmission coefficients of the air sample and of the sample–air interfaces, respectively. We replace the complex refractive index $\tilde{n}(\nu) = n(\nu) - i\kappa(\nu)$ into the Fresnel transmission coefficients and then obtain

$$T(\nu) = \frac{4(n-i\kappa)}{(1+(n-i\kappa))^2} \cdot \exp(-\alpha \cdot d) \cdot \exp\Big(-i\frac{2\pi\nu(n-1)\cdot d}{c}\Big), \quad (2)$$

where $\alpha = \frac{2\pi\nu}{c}\kappa$ is the absorption coefficient. Solving Eq. (2) numerically allows us to determine the complex refractive index from the experimental measurements. Due to the moderate attenuation of the THz pulse inside the sample and $\kappa \ll n$, thus n can be directly determined by the phase delay of the $T(\nu)$ as $n(\omega) = \Delta\varphi \cdot \frac{c}{2\pi\nu d} + 1$, and $\alpha(\omega) = \frac{2}{d} \cdot \ln[\frac{4n(\nu)}{A(\nu)\cdot((n(\nu)+1))^2}]$.[28,29] Furthermore, the complex permittivity is given by $\widetilde{\varepsilon} = \varepsilon_r + i\varepsilon_i$, where $\varepsilon_r = n^2 - \kappa^2$, $\varepsilon_i = 2n\kappa$, and ε_r is also known as the dielectric constant, indicating that the amount of energy from an external electrical field can be stored in the material. However, ε_i is a measure of the amount of energy loss from the material, which is mainly attributed to the bound charge and dipole relaxation phenomena.

Figure 2(d) shows the refractive index and absorption coefficient of the TSAG crystal in the frequency range 0.4–1.4 THz, obtained at room temperature, using the above-mentioned procedure. Both the refractive index and the absorption coefficient increase gradually with the frequency. The mean value of the refractive index is nearly a constant of 3.2 within our THz frequency range, which can be used to calculate the THz surface reflectance of the sample. In addition, it should be noted that the quartz window of the cryostat will limit the whole frequency range up to around 1.4 THz, as shown in Figs. 2(a) and 2(c). The signal-to-noise ratio also drops rapidly above 1.4 THz. In further studies, we will attempt to improve the bandwidth of the THz-TDS measurement with high accuracy.

Figure 3(a) shows the THz transmission measurements at the selected temperatures. When the temperature is increased, the time delay of the THz pulse is slightly increased, as shown by the dashed line, which is due to the increase of the group velocity of the THz pulse. In addition, it can also be found that the amplitude of the THz pulses increases with the temperature. It should be mentioned that, due to the thermal expansion of the sample, the thickness of the sample depends on the temperature. However, we cannot determine the thickness of the sample as it was mounted inside the cryostat. However, the thermal expansion coefficient measured for TSAG is around $8.4 \times 10^{-6}\,\mathrm{K}^{-1}$. Thus we find that a variation of the thickness for the sample in the measured temperature range is less than 2%, which has a negligible effect on the refractive index.

Figures 3(b) and 3(c) show the frequency spectra of the complex refractive index range from 0.4 to 1.4 THz at different temperatures. As shown by the arrow, the values of $\alpha(\nu)$ of TSAG are found to be temperature dependent, which is increasing to higher values with the temperature. As the temperature rises, disorders are created in the lattice and the mobility of the ions increases. The values of n in the temperature range from 100 to 300 K for several selected frequencies of 0.8 THz, 1.0 THz and 1.2 THz are shown in the inset of Fig. 3(b). We find that n increases slightly with the temperature. Our results suggest that n is associated to the thermal motion of dipoles, which cannot orient themselves at low temperatures.[30,31]

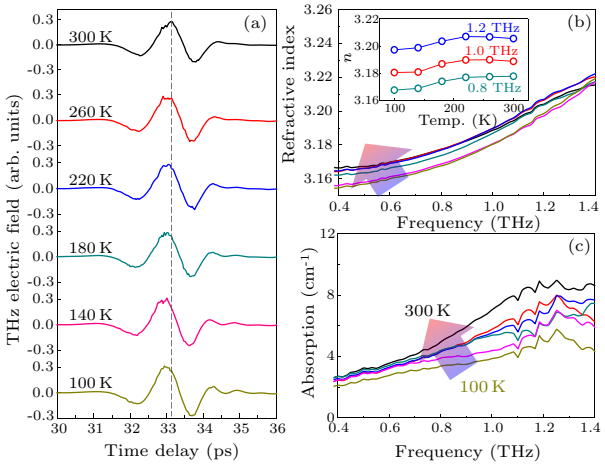

Fig. 3. (a) The THz transients transmitted through the TSAG crystal at different temperatures. Frequency dependences of (b) refractive index (n) and (c) absorption coefficient of TSAG from 100 to 300 K (as shown by the arrow), obtained from the time-domain THz waveforms. Inset of (b): Plot of n at 0.8, 1.0 and 1.2 THz as a function of different temperatures.

The temperature dependence of n of TSAG can be described in terms of a temperature coefficient

$$\tau_n = \frac{1}{n} \cdot \frac{dn(T)}{dT}, \quad (3)$$

where n is the refractive index measured at room temperature. By fitting with Eq. (3), the τ_n data are obtained to be $(18.0 \pm 3.2) \times 10^{-6}\,\mathrm{K}^{-1}$@0.8 THz, $(16.0 \pm 4.4) \times 10^{-6}\,\mathrm{K}^{-1}$@1.0 THz and $(14.8 \pm 4.8) \times 10^{-6}\,\mathrm{K}^{-1}$@1.2 THz, indicating the relative change of n as the temperature is changed. The temperature coefficients τ_n are plotted as a function of THz frequencies in Fig. 4. In contrast to TiO_2 and (Zr,Sn)TiO_3,[27] τ_n of TSAG is positive in the investigated frequency range. In addition, τ_n of TSAG is much smaller than that of Al_2O_3, showing a thermal stability for the TSAG crystal.

Finally, Fig. 5(a) shows the real and imaginary parts of the permittivity versus the frequency for different temperatures. The value of ε_r increases from ~10.0 to ~10.4 with the frequency increasing from 0.4 to 1.4 THz. Similar to the refractive index, ε_r increases with the temperature, while ε_i is relatively small and featureless within our present THz range. We have further calculated the loss tangent for the engineering

application. The loss tangent is defined as the ratio of the imaginary part to the real part of the complex permittivity, $\tan\delta = \frac{\varepsilon_i}{\varepsilon_r}$, which is used to describe the dielectric loss. As represented in Fig. 5(b), the loss tangent of the TSAG crystal is comparably low, which slightly increases with the temperature. The difference between the $\tan\delta$ values at 300 K and at 100 K is less than 0.005, for almost all frequencies, as shown in Fig. 5(c). The loss tangent of TSAG is less than the value of high-k materials such as TiO_2,[27] while it is similar to the value of Al_2O_3 and orthorhombic perovskite $YAlO_3$, which is reported to be 0.01–0.02 at frequencies from 1.5 to 3.0 THz.[32] The weak loss means that TSAG crystals are good candidates for high-permittivity insulation materials in optoelectronic devices in THz frequency ranges.

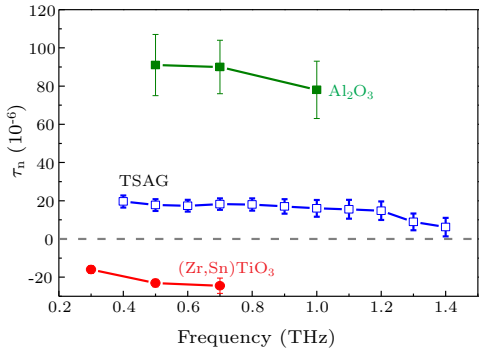

Fig. 4. Temperature coefficient τ_n of the refractive index of the TSAG crystal, compared with zirconium-tin-titanate (Zr,Sn)TiO_3, and alumina (Al_2O_3) in the range 0.3–1.4 THz, which are taken from Ref. [27].

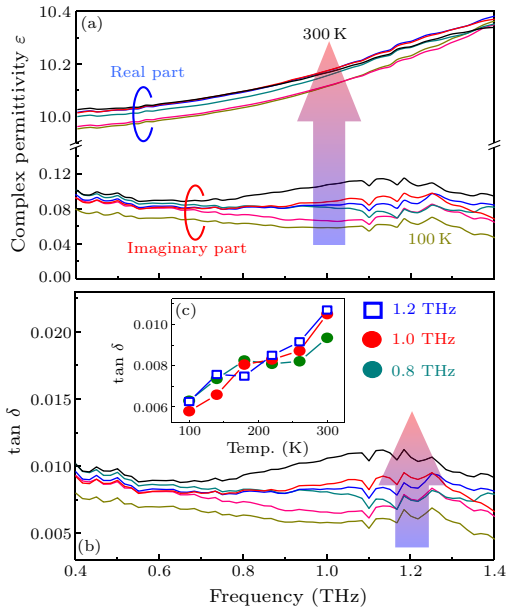

Fig. 5. (a) Permittivity and (b) loss tangent of the TSAG crystal measured at different temperatures. (c) The loss tangent at 0.8, 1.0 and 1.2 THz versus temperature.

In summary, we have used time-domain THz spectroscopy to study the temperature-dependent THz dielectric response of paramagnetic TSAG crystals from 0.4 THz to 1.4 THz. The experimental results show that the values of real and imaginary permittivity are found to increase with the frequency and the temperature. The present results demonstrate that TSAG is designed to provide high thermal stability. Our work enables researchers to use the temperature-dependent permittivity of TSAG to design optoelectronic devices in THz frequency more accurately.[33,34] Finally, our findings also have a prospect for applications of the THz spectroscopy to other magnetic dielectric materials and magnonic metamaterials.[35]

References

[1] Kirilyuk A et al 2010 *Rev. Mod. Phys.* **82** 2731
[2] Jin Z M et al 2010 *Appl. Phys. Lett.* **96** 201108
[3] Stupakiewicz A et al 2017 *Nature* **542** 71
[4] Mikhaylovskiy R V et al 2012 *Phys. Rev. B* **86** 100405
[5] Jin Z M et al 2011 *Acta Phys. Sin.* **60** 087803 (in Chinese)
[6] Bakunov M I et al 2007 *Phys. Rev. B* **76** 085346
[7] Gorelov S D et al 2012 *Phys. Rev. B* **88** 220411(R)
[8] Subkhangulov R R et al 2016 *Nat. Photon.* **10** 111
[9] Lin X et al 2008 *Acta Phys. Sin.* **67** 2378 (in Chinese)
[10] Riordan J A et al 1997 *Appl. Phys. Lett.* **71** 1452
[11] Qiu H S et al 2018 *Opt. Lett.* **43** 1658
[12] Luszcz K, Bonvin E and Novotny L 2018 *Appl. Phys. Lett.* **113** 111103
[13] Chen X, Zhang W H, Wan Q P, Guo F Y, Zhuang N F, Fu H, Xie X T and Chen J Z 2014 *Opt. Mater.* **37** 188
[14] Lu J Y, Fu C and Chen J Z 2011 *Appl. Opt.* **50** 116
[15] Guo F Y, Ru J J, Li H Z, Zhuang N F, Zhao B and Chen J Z 2008 *J. Cryst. Growth* **310** 4390
[16] Kagamitani Y, Pawlak D A, Sato H, Yoshikawa A, Machida H and Fukuda T 2002 *Jpn. J. Appl. Phys.* **41** 6020
[17] Ding S, Zhang Q, Liu W, Luo J, Sun G and Sun D 2018 *J. Cryst. Growth* **483** 110
[18] Mironov E A and Palashov O V 2014 *Opt. Express* **22** 23226
[19] Víllora E G, Molina1 P, Nakamura M, Shimamura K, Hatanaka T, Funaki A and Naoe K 2011 *Appl. Phys. Lett.* **99** 011111
[20] Shi L J, Guo L W, Wei Q K, Song C G, Hu X L, Zhuang N F, Lin S K and Chen J Z 2013 *J. Synth. Cryst.* **42** 1735
[21] Ding J X, Jin W Z, Chen Q M, Hou C H, Yu Y, Su L B, Li C, Zeng F M and Wu A H 2018 *Opt. Mater. Express* **8** 2880
[22] Mikhaylovskiy R V, Hendry E, Ogrin F Y and Kruglyak V V 2013 *Phys. Rev. B* **87** 094414
[23] Neu J and Schmuttenmaer C A 2018 *J. Appl. Phys.* **124** 231101
[24] Hangyo M, Tani M and Nagashima T 2005 *J. Infrared Millimeter Terahertz Waves* **26** 1661
[25] Starobor A V, Snetkov I L and Palashov O V 2018 *Opt. Lett.* **43** 3774
[26] Starobor A, Yasyhara R, Snetkov I, Mironov E and Palashov O 2015 *Opt. Mater.* **47** 112
[27] Berdel K, Rivas J G, Bolívar P H, Maagt P and Kurz H 2005 *IEEE Trans. Microwave Theory Tech.* **53** 1266
[28] Sun Y M, Mao Z L, Hou B L, Liu G Q and Wang L 2007 *Chin. Phys. Lett.* **24** 414
[29] Han X W, Hou L, Yang L, Wang Z Q, Zhao M M and Shi W 2016 *Chin. Phys. Lett.* **33** 120701
[30] Ertuğrul R and Tataroğlu A 2012 *Chin. Phys. Lett.* **29** 077304
[31] Sattar A A and Rahman S A 2003 *Phys. Stat. Sol. (a)* **200** 415
[32] Morimoto T, Kuroda Y and Ohki Y 2017 *Jpn. J. Appl. Phys.* **56** 102601
[33] Kriegel I and Scotognella F 2017 *Optik* **142** 249
[34] Adachi M, Yamahara H, Kawabe S, Matsui H and Tabata H 2014 *Phys. Rev. B* **89** 205124
[35] Kruglyak V V, Demokritov S O and Grundler D 2010 *J. Phys. D* **43** 264001